# Ordered Arrangement of Planar Faults with Pico-Scale Perfection in Titanium Oxide Natural Superlattice

*Shunta Harada[1,2,3*], Naoki Kosaka[2], Miho Tagawa[1,2], Toru Ujihara[1,2,4]*

[1] Center for Integrated Research of Future Electronics (CIRFE), Institute of Materials and Systems for Sustainability (IMaSS), Nagoya University, Furo-cho, Chikusa-ku, Nagoya 464-8601, Japan

[2] Department of Materials Process Engineering, Nagoya University, Furo-cho, Chikusa-ku, Nagoya 464-8603, Japan

[3] PRESTO, Japan Science and Technology Agency, 4-1-8 Honcho, Kawaguchi, Saitama 332-0012, Japan

[4] GaN Advanced Device Open Innovation Laboratory (GaN-OIL), National Institute of Advanced Industrial Science and Technology (AIST), Nagoya University, Furo-cho, Chikusa-ku, Nagoya 464-8601, Japan

Keywords

coherent thermal transport, natural superlattice, crystallographic shear structure, specularity parameter

**Abstract**

Coherent control of thermal phonons by atomic scale periodic structures is of great interest due to the potential for advanced thermal management. However, the coherence is easily broken by interface roughness and interfaces with sub-atomic scale perfection, which have never been achieved even by advanced synthesis of artificial superlattice thin films, are strongly needed. Here we demonstrated that the ordered arrangement of planar faults in titanium oxide natural superlattices has pico-scale structural perfection. HAADF-STEM observation revealed that the average periodicity disorder was 36 pm for interface spacings of 2.64-2.85 nm, and the interface roughness was estimated to be 15 pm. Calculation of the specularity parameter indicates that the interface behaves coherently for phonons with frequency less than 23 THz, which includes almost all phonons in rutile $TiO_2$. Coherent phonon transport should become apparent in the titanium oxide NSL system owing to these smooth interfaces, whose roughness is one order of magnitude lower than that in artificial superlattice thin films.

## Introduction

Control of heat conduction by nanoscale periodic structures through the manipulation of phonons as coherent waves is of great interest for the realization of advanced thermal management, which is different from the case of diffuse transport following Fourier's law[1–8]. Coherent thermal transport in nanoscale periodic structures has been mainly investigated using nanostructures

fabricated by lithography methods (called phononic crystals)[3,9–11], nanowires[12,13], nanodots[14,15] or artificial superlattice thin films[16–23]. For the demonstration of coherent heat conduction, especially above room temperature, it is necessary to fabricate an interface having nanoscale or sub-nanoscale periodicity with high perfection. Superlattices are the ideal system for the realization and understanding of coherent heat conduction, and recently coherent heat conduction was reported in several artificial superlattices such as GaAs/AlAs grown by metal-organic chemical vapor deposition (MOCVD), $SrTiO_3/CaTiO_3$ grown by molecular beam epitaxy (MBE) and TiN/(Al, Sc)N grown by reactive dc-magnetron sputtering[18,21,24] . Although smooth interfaces were reported to be achieved in the superlattices, the realization of coherent interfaces for thermal phonons is still challenging, since sub-atomic scale or even pico-scale perfection is necessary. In order to achieve interfaces with such high perfection, a disadvantage of artificial superlattices is that the growth process is unavoidably nonequilibrium thermodynamically. Natural superlattices (NSLs), in which multi-layered structures are spontaneously formed as thermodynamically stable phases, are one good choice for the realization of coherent interfaces for thermal phonons.

Among various kinds of layered materials including NSLs[25–30], we focused on crystallographic shear (CS) structures introduced in some reduced $TiO_2$ (rutile) because of the tunability of the atomic-scale periodic structures. The homologous series of titanium oxides with CS structures expressed as $Ti_nO_{2n-1}$ ($n$ = 4, 5,…) contains ordered arrangements of planar faults called CS planes, on which atoms are displaced from their mother rutile positions by a certain vector called the CS vector and oxygen deficiency takes place[31–33]. The CS structure can compensate for the oxygen deficiency by changing the spacing of the CS planes. Therefore, it is possible to tune the interval of the CS planes in the mother rutile structure by changing the composition (oxygen deficiency). The CS structures of titanium oxides have been thoroughly

investigated and have been reported to change depending on the composition. When $n$ in $Ti_nO_{2n-1}$ is smaller than 10, the CS plane and vector are $(121)_{rutile}$ and $1/2[0\text{-}11]_{rutile}$[31,34], while the CS plane is reported to be $(132)_{rutile}$ when $n$ is greater than around 15, and the orientation of the CS plane is reported to be between $(121)_{rutile}$ and $(132)_{rutile}$ in the intermediate compositions[33,35].

In the present study, we investigated the structural perfection of $(132)_{rutile}$ CS structures in slightly reduced titanium oxides to reveal whether the CS planes act as coherent interfaces for thermal phonons.

**Crystallographic shear structure in slightly reduced rutile**

Bursil and Hyde[35] identified that the CS plane and vector for slightly reduced rutile with $Ti_nO_{2n-1}$ with the value of $n$ ranging from 15 to 36 are $(132)_{rutile}$ and $1/2[0\text{-}11]_{rutile}$. A schematic illustration of the ideal atomic arrangement of titanium oxides with $(121)_{rutile}$ and $(132)_{rutile}$ CS planes as well as the $(011)_{rutile}$ anti-phase boundary (APB) with the displacement of $1/2[0\text{-}11]_{rutile}$ are shown in Fig. 1. Since the $1/2[0\text{-}11]_{rutile}$ vector, which is the CS vector or the displacement vector for the $(011)_{rutile}$ APB, corresponds to an oxygen atom site displaced to the next site, the oxygen arrangements are not disturbed on the CS plane. On the other hand, the arrangement of titanium atoms is disturbed because the $1/2[0\text{-}11]_{rutile}$ vector corresponds to the displacement of a titanium atom site to the interstitial site in the oxygen octahedron. Of importance to note in Fig. 1 is that the $(132)_{rutile}$ CS plane can be regarded as an alternative arrangement of the CS $(121)_{rutile}$ plane and the $(011)_{rutile}$ APB. Recently, the atomic arrangement of titanium columns in zirconium-doped $Ti_{10}O_{19}$ was directly observed by high-angle annular dark-field scanning transmission electron

microscopy (HAADF-STEM)[28]. Therefore, the direct observation of titanium atom columns by HAADF-STEM can be used to evaluate the structural perfection of the CS planes.

The stacking sequence of the $(121)_{rutile}$ and $(132)_{rutile}$ planes can be expressed as -**BAB BAB BAB**-, where **A** denotes a titanium layer (**A** =Ti) and **B** denotes an oxygen layer (**B** =O). The presence of a CS plane (denoted as *****) changes the sequence to -**BAB BA*BAB**-. If a CS plane is introduced every $n$ titanium layers (**A**), the composition is described as $Ti_nO_{2n-1}$. The CS vector $1/2[0\text{-}11]_{rutile}$ has a component normal to the $(132)_{rutile}$ CS plane, and the ideal spacing of the $(132)_{rutile}$ CS planes ($D_{CS}$) for $Ti_nO_{2n-1}$ is expressed as follows:

$$D_{CS} = d_{132} (n - 1/2), \quad (1)$$

where $d_{132}$ (= 0.1036 nm) stands for the interplanar distance of $(132)_{rutile}$[35]. Thus, the spacing of the CS plane can be estimated from the HAADF-STEM observation of titanium atom columns by counting the number of titanium layers between CS planes.

When the CS planes are introduced into the mother rutile structure, a series of superlattice reflection spots along the reciprocal lattice vector corresponding to the CS plane (along $\boldsymbol{g}(132)_{rutile}$) appear at the positions corresponding to $n$. For example, when $n$ is 20, twenty equally spaced superlattice spots are observed between the transmitted beam spot and that corresponding to the $(132)_{rutile}$ CS plane in a selected area electron diffraction (SAED) pattern. Thus, the spacing of the CS plane can also be evaluated by analysis of the SAED patterns. In the present study, we investigated the structure and periodicity of the CS planes introduced in slightly reduced rutile by HAADF-STEM observation as well as SAED patterns.

## Experimental procedure

A rutile $TiO_2$ single crystal grown by the Verneuil method was reduced by annealing at 1573 K for 24 h in vacuo ($<1\times10^{-4}$ Pa) with titanium metal. The atomic structure was examined by transmission electron microscopy (TEM) as well as STEM using a JEOL JEM-ARM200 transmission electron microscope operated at 200 kV. The specimens for (S)TEM observations were prepared by Ar ion milling using a JEOL Ion Slicer (EM-09100IS).

## Results

Figure 2 shows the SAED patterns taken from the prepared specimen along the $[1\text{-}11]_{rutile}$ direction. A line of superlattice spots indicating the occurrence of an ordered arrangement of the CS planes is directed along $(132)_{rutile}$. In Fig. 2(a) and the magnified image of Fig. 2(c), superlattice spots appear at the positions corresponding to $n = 26$. The positions of superlattice spots were different depending on the positions of the selected area aperture. At some positions, the SAED pattern is a superposition of those from different spacings of CS planes ($n = 27$ and 28) as shown in Fig. 2(b) and the magnified image of Fig. 2(d). From this specimen, we observed superlattice spots at intervals corresponding to 26, 27 and 28 times the interplanar distance of $(132)_{rutile}$, which indicates that the composition of the specimen is estimated as $TiO_{1.962\sim1.964}$. Table 1 summarizes the compositions and the spacings of the CS planes ($D_{CS}$) calculated by Eq. (1) for the observed phases. The coexistence of at least three phases ($Ti_{26}O_{51}$, $Ti_{27}O_{53}$ and $Ti_{28}O_{55}$) indicates that the specimen was heterogeneous and did not reach complete thermal equilibrium. Bursil and Hyde also reported that slightly reduced rutile was "strikingly" heterogeneous[35], and it is difficult to obtain single-phase $Ti_nO_{2n-1}$ with values of $n$ ranging from 15 to 36 by reduction annealing. Although the spacing

of the CS plane depends on the position in the sample, it seems that the CS plane spacing was homogeneous at least within the area where the SAED pattern was taken (about 200 nm length scale). In the SAED patterns, the superlattice spots were sharp and no streaks were noticed. This implies that the CS spacing is not disturbed within each phase.

Figure 3 shows HAADF-STEM images of $Ti_{28}O_{55}$ along $[1\text{-}11]_{rutile}$. In the HAADF-STEM images, titanium atom columns are imaged as bright spots, while oxygen atom columns are not imaged individually. The arrangement of titanium atom columns deviates on the $(132)_{rutile}$ CS planes, and the HAADF-STEM observation agreed with the reported CS structure with CS vector of almost $1/2[0\text{-}11]_{rutile}$[35]. From the HAADF-STEM images, the interplanar distance of the CS planes can be evaluated by counting the number of $(132)_{rutile}$ titanium layers ($n$), as shown in Fig. 3(b) (the value of $n$ is evidently 28. From STEM observations over a wider range, the distribution of the interplanar distance of the CS planes can be estimated by counting the $(132)_{rutile}$ titanium layers. In Fig. 3(c), for example, only the interplanar distance corresponding to $n$ = 28 was observed. However, the interplanar distance was not always the same, with different values of $n$ sometimes appearing. Table 2 summarizes the standard deviation for the values of $n$ and the interplanar distance of the CS plane evaluated from the HAADF-STEM images taken from $Ti_{26}O_{51}$, $Ti_{27}O_{53}$ and $Ti_{28}O_{55}$ in different positions, and a histogram of the values of $n$ is shown in Fig. 4. The standard deviation of the value of $n$ was estimated as 0.35. In other words, the standard deviation of the spacing of the CS planes was as small as 36 pm. The nanoscale ordered arrangement of the CS planes in titanium oxides possesses periodicity with subatomic scale perfection.

As can be seen in Figs. 3(a) and 3(b), the $(132)_{rutile}$ CS plane was indeed an alternative arrangement of the $(121)_{rutile}$ CS plane and the $(011)_{rutile}$ APB, which was rarely disturbed.

However, in some positions, the atomic arrangement was disordered, as shown in Fig. 5(a). Compared with the normal atomic arrangement shown in Fig. 5(b), one of the titanium atomic column sites on the CS plane splits into two sites with weak contrast (Fig. 5(c)). The intensity profile measured along the two titanium atomic column sites X (X') and Y (Y') in Figs. 5(b) and 5(c) is shown in Fig. 6. Evidently one titanium atomic column site (A-site) is split into two titanium atomic column sites (A-site and B-site). If these two sites are separately illustrated as shown in Fig. 7, one can easily notice that the site splitting in the HAADF-STEM image indicates that CS planes with positions different by one $(132)_{rutile}$ titanium layer are duplicated along the incident direction.

The value of average roughness ($R_a$) was estimated from the maximum height ($R_z$) by using the formula $R_a = 4R_z$, which is completely established in the case of repetition of the same zigzag shape and is sometimes used for the estimation of $R_a$ for machined surfaces[29]. The maximum heights ($R_z$) for a $(132)_{rutile}$ CS plane with ideal structure and one with site splitting were $0.5d_{132}$ and $1.5d_{132}$, respectively. The values of $R_a$ estimated from the formula are tabulated in Table 3. By measuring the length of the CS plane with site splitting in HAADF-STEM image, the average roughness was estimated to be only 15 pm.

**Discussion**

The coherence of interfaces is often discussed by using the specularity parameter $p$, which plays an important role in various models for boundary scattering[17,37–39]. An incident phonon is coherently scattered by a perfectly specular interface ($p = 1$), while completely diffuse scattering occurs on an interface with $p = 0$ (the so-called Casimir limit). Ziman originally derived a simple

expression for the specularity parameter of phonons depending on the frequency ($f$) for a random rough interface as a function of the root mean square (RMS) value for roughness ($R$), assuming an infinite correlation length and normal incidence of phonons to the interface as follows[40];

$$p(f) = exp(-16\pi^2(\frac{Rf}{v})^2), \quad (2)$$

where $v$ is the group velocity of phonons. Maire et al. adopted the following effective roughness ($R_{eff}$) considering not only the roughness of the interface ($\sigma$) but also the periodicity disorder ($\xi$) in the following expression:

$$R_{eff} = \sqrt{\sigma^2 + (0.5\xi)^2}. \quad (3)$$

By using the estimated values from the HAADF-STEM data ($\sigma$ = 15 pm and $\xi$ = 36 pm), the effective roughness for the periodic arrangement of the CS planes in the titanium oxide NSL was estimated to be 23 pm. Figure 8 shows the specularity parameters as a function of frequency calculated using eq. (2). Wagner et al. suggested that a specularity parameter larger than 0.3 constitutes a criterion for a coherent interface, and a specularity parameter smaller than 0.01 is a criterion for a noncoherent interface[10]. Following these criteria, it is expected that the CS planes behave as coherent interfaces for the phonons with frequency less than 23 THz. Considering that the highest phonon mode frequency (top of the optical mode) in rutile $TiO_2$ was reported as around 25 THz[41,42], the CS planes are considered to behave as coherent interfaces for almost all thermal phonons. Table 4 summarizes the periodicity disorder and the roughness of the interface for the present results and other materials, including artificial superlattice thin films and phononic crystals[11,43,44]. The interface roughness for the NSL in the present study was one order of magnitude smaller than that for the artificial superlattice with similar period, which should result in coherent phonon transport becoming apparent.

Although the CS planes of the titanium oxide NSLs in the present study possess high structural perfection, the effect of coherent phonon transport on the thermal conductivity was not observed, and rather incoherent aspects of the interface emerged in previous studies using hot-pressed polycrystalline ceramics[33,45]. This implies that the structural perfection of the CS plane depends on the synthetic method. Recently, Teramoto et al. reported the atomic arrangement of a zirconium-doped titanium oxide NSL with $(132)_{rutile}$ CS planes prepared by sintering and hot-pressing at 1473 K[28]. In their paper, the contrast of the titanium atom columns near the CS plane was weaker than the other columns and site-splitting of the titanium column was frequently observed, indicating the occurrence of not only one titanium layer deviation as shown in Fig. 5(b) but also deviations of two or more $(132)_{rutile}$ titanium layers near the CS plane, which would lead to an increase in the roughness of the CS plane. Synthesis by sintering at low temperature may be insufficient for the formation of CS planes with high perfection, as achieved in the present study. Another possible issue is the short mean free path of phonons in rutile $TiO_2$ above room temperature. The evaluated mean free path for phonons in a titanium oxide NSL polycrystal assuming the Debye model was reported as 0.8 nm at room temperature, and even shorter at higher temperature. Coherent thermal transport is expected to become apparent when the mean free path is longer than the spacing of the CS plane. Thus, CS planes with short spacing and measurement of thermal conductivity at low temperature are preferable for the investigation of coherent phonon transport.

## Conclusion

The atomic structure and structural perfection of an ordered arrangement of CS planes in titanium oxide NSLs were investigated by use of a rutile single crystal that was slightly reduced by high temperature annealing in vacuum. The results obtained are summarized as follows:

(1) Coexistence of at least three phases ($Ti_{26}O_{51}$, $Ti_{27}O_{53}$ and $Ti_{28}O_{55}$) with an ordered arrangement of the $(132)_{rutile}$ CS plane with different spacings was observed in the prepared specimen by means of SAED patterns as well as HAADF-STEM images.

(2) The average standard deviation of the spacing of the CS planes was only 36 pm and the interface roughness for the CS planes was estimated to 15 pm, which is one order magnitude smaller than that for the interface of artificial superlattices.

(3) Calculation of the specularity parameters from the effective roughness estimated from the results of the HAADF-STEM observation suggested that the CS planes behave as coherent interfaces for phonons with the frequency less than 23 THz, which is almost all phonons in rutile $TiO_2$.

(4) Coherent phonon transport, which has never been clearly demonstrated experimentally, is expected to be realized in titanium oxide NSLs owing to their low interface roughness.

AUTHOR INFORMATION

**Corresponding Author**

* Shunta Harada

Institute of Materials and Systems for Sustainability, Nagoya University, Furo-cho, Chikusa-ku, Nagoya, 464-8601 Japan; E-mail: shunta.harada@nagoya-u.jp

**Author Contributions**

S. H. conceived and designed the experiments and the analysis. S. H. carried out the experiments and the analysis with N. K. The experimental data and analysis were discussed by all authors. The manuscript was written by S. H. in discussion with all the authors. All authors have given approval for the final version of the manuscript.

**Note**

The authors declare no competing financial interest.

ACKNOWLEDGMENT

This work was partly supported by JST PRESTO (JPMJPR18I8) and Grant-in-Aid for Scientific Research (B) from MEXT (18H01733).

SUPPORTING INFROMATION

Procedure of averaging HAADF-STEM image and raw images before the averaging procedure.

REFERENCES

(1) Narayanamurti, V. Phonon Optics and Phonon Propagation in Semiconductors. *Science* **1981**, *213* (4509), 717–723. https://doi.org/10.1126/science.213.4509.717.

(2) Simkin, M. V.; Mahan, G. D. Minimum Thermal Conductivity of Superlattices. *Phys. Rev. Lett.* **2000**, *84* (5), 927–930. https://doi.org/10.1103/PhysRevLett.84.927.

(3) Yu, J. K.; Mitrovic, S.; Tham, D.; Varghese, J.; Heath, J. R. Reduction of Thermal Conductivity in Phononic Nanomesh Structures. *Nat. Nanotechnol.* **2010**, *5* (10), 718–721. https://doi.org/10.1038/nnano.2010.149.

(4) Dechaumphai, E.; Chen, R. Thermal Transport in Phononic Crystals: The Role of Zone Folding Effect. *J. Appl. Phys.* **2012**, *111* (7). https://doi.org/10.1063/1.3699056.

(5) Maldovan, M. Sound and Heat Revolutions in Phononics. *Nature* **2013**, *503* (7475), 209–217. https://doi.org/10.1038/nature12608.

(6) Maldovan, M. Phonon Wave Interference and Thermal Bandgap Materials. *Nat. Mater.* **2015**, *14* (7), 667–674. https://doi.org/10.1038/nmat4308.

(7) Nomura, M.; Shiomi, J.; Shiga, T.; Anufriev, R. Thermal Phonon Engineering by Tailored Nanostructures. *Jpn. J. Appl. Phys.* **2018**, *57* (8), 080101. https://doi.org/10.7567/JJAP.57.080101.

(8) Liao, Y.; Shiga, T.; Kashiwagi, M.; Shiomi, J. Akhiezer Mechanism Limits Coherent Heat Conduction in Phononic Crystals. *Phys. Rev. B* **2018**, *98* (13), 134307. https://doi.org/10.1103/PhysRevB.98.134307.

(9) Alaie, S.; Goettler, D. F.; Su, M.; Leseman, Z. C.; Reinke, C. M.; El-Kady, I. Thermal Transport in Phononic Crystals and the Observation of Coherent Phonon Scattering at Room Temperature. *Nat. Commun.* **2015**, *6*. https://doi.org/10.1038/ncomms8228.

(10) Wagner, M. R.; Graczykowski, B.; Reparaz, J. S.; El Sachat, A.; Sledzinska, M.; Alzina, F.; Sotomayor Torres, C. M. Two-Dimensional Phononic Crystals: Disorder Matters. *Nano Lett.* **2016**, *16* (9), 5661–5668. https://doi.org/10.1021/acs.nanolett.6b02305.

(11) Maire, J.; Anufriev, R.; Yanagisawa, R.; Ramiere, A.; Volz, S.; Nomura, M. Heat Conduction Tuning by Wave Nature of Phonons. *Sci. Adv.* **2017**, *3* (8). https://doi.org/10.1126/sciadv.1700027.

(12) Wingert, M. C.; Chen, Z. C. Y.; Dechaumphai, E.; Moon, J.; Kim, J. H.; Xiang, J.; Chen, R. Thermal Conductivity of Ge and Ge-Si Core-Shell Nanowires in the Phonon Confinement Regime. *Nano Lett.* **2011**, *11* (12), 5507–5513. https://doi.org/10.1021/nl203356h.

(13) Chen, J.; Zhang, G.; Li, B. Impacts of Atomistic Coating on Thermal Conductivity of Germanium Nanowires. *Nano Lett.* **2012**, *12* (6), 2826–2832. https://doi.org/10.1021/nl300208c.

(14) Luckyanova, M. N.; Mendoza, J.; Lu, H.; Song, B.; Huang, S.; Zhou, J.; Li, M.; Dong, Y.; Zhou, H.; Garlow, J.; Wu, L.; Kirby, B. J.; Grutter, A. J.; Puretzky, A. A.; Zhu, Y.; Dresselhaus, M. S.; Gossard, A.; Chen, G. Phonon Localization in Heat Conduction. *Sci. Adv.* **2018**, *4* (12), eaat9460. https://doi.org/10.1126/sciadv.aat9460.

(15) Taniguchi, T.; Terada, T.; Komatsubara, Y.; Ishibe, T.; Konoike, K.; Sanada, A.; Naruse, N.; Mera, Y.; Nakamura, Y. Phonon Transport in the Nano-System of Si and SiGe Films with Ge Nanodots and Approach to Ultralow Thermal Conductivity. *Nanoscale* **2021**, *13* (9), 4971–4977. https://doi.org/10.1039/d0nr08499a.

(16) Yang, B.; Chen, G. Partially Coherent Phonon Heat Conduction in Superlattices. *Phys. Rev. B* **2003**, *67* (19), 195311. https://doi.org/10.1103/PhysRevB.67.195311.

(17) Koh, Y. K.; Cao, Y.; Cahill, D. G.; Jena, D. Heat-Transport Mechanisms in Superlattices. *Adv. Funct. Mater.* **2009**, *19* (4), 610–615. https://doi.org/10.1002/adfm.200800984.

(18) Luckyanova, M. N.; Garg, J.; Esfarjani, K.; Jandl, A.; Bulsara, M. T.; Schmidt, A. J.; Minnich, A. J.; Chen, S.; Dresselhaus, M. S.; Ren, Z.; Fitzgerald, E. A.; Chen, G. Coherent Phonon Heat Conduction in Superlattices. *Science* **2012**, *338*, 936–939. https://doi.org/10.1126/science.1225549.

(19) Luckyanova, M. N.; Johnson, J. A.; Maznev, A. A.; Garg, J.; Jandl, A.; Bulsara, M. T.; Fitzgerald, E. A.; Nelson, K. A.; Chen, G. Anisotropy of the Thermal Conductivity in GaAs/AlAs Superlattices. *Nano Lett.* **2013**, *13* (9), 3973–3977. https://doi.org/10.1021/nl4001162.

(20) Ravichandran, J.; Yadav, A. K.; Cheaito, R.; Rossen, P. B.; Soukiassian, A.; Suresha, S. J.; Duda, J. C.; Foley, B. M.; Lee, C. H.; Zhu, Y.; Lichtenberger, A. W.; Moore, J. E.; Muller, D. A.; Schlom, D. G.; Hopkins, P. E.; Majumdar, A.; Ramesh, R.; Zurbuchen, M. A. Crossover from Incoherent to Coherent Phonon Scattering in Epitaxial Oxide Superlattices. *Nat. Mater.* **2014**, *13* (2), 168–172. https://doi.org/10.1038/nmat3826.

(21) Saha, B.; Koh, Y. R.; Feser, J. P.; Sadasivam, S.; Fisher, T. S.; Shakouri, A.; Sands, T. D. Phonon Wave Effects in the Thermal Transport of Epitaxial TiN/(Al,Sc)N Metal/Semiconductor Superlattices. *J. Appl. Phys.* **2017**, *121* (1), 015109. https://doi.org/10.1063/1.4973681.

(22) Hiroi, S.; Nishino, S.; Choi, S.; Seo, O.; Kim, J.; Chen, Y.; Song, C.; Tayal, A.; Sakata, O.; Takeuchi, T. Phonon Scattering at the Interfaces of Epitaxially Grown $Fe_2VAl$/W and $Fe_2VAl$/Mo Superlattices. *J. Appl. Phys.* **2019**, *125* (22), 225101. https://doi.org/10.1063/1.5080976.

(23) Choi, S.; Hiroi, S.; Inukai, M.; Nishino, S.; Sobota, R.; Byeon, D.; Mikami, M.; Minamitani, E.; Matsunami, M.; Takeuchi, T. Crossover in Periodic Length Dependence

of Thermal Conductivity in 5d Element Substituted $Fe_2VAl$ -Based Superlattices. *Phys. Rev. B* **2020**, *102* (10), 104301. https://doi.org/10.1103/PhysRevB.102.104301.

(24) Ravichandran, J.; Yadav, A. K.; Cheaito, R.; Rossen, P. B.; Soukiassian, A.; Suresha, S. J.; Duda, J. C.; Foley, B. M.; Lee, C.-H.; Zhu, Y.; Lichtenberger, A. W.; Moore, J. E.; Muller, D. A.; Schlom, D. G.; Hopkins, P. E.; Majumdar, A.; Ramesh, R.; Zurbuchen, M. A. Crossover from Incoherent to Coherent Phonon Scattering in Epitaxial Oxide Superlattices. *Nat. Mater.* **2014**, *13* (2), 168–172. https://doi.org/10.1038/nmat3826.

(25) Gomyo, A.; Suzuki, T.; Iijima, S. Observation of Strong Ordering in $Ga_xIn_{1-x}P$ Alloy Semiconductors. *Phys. Rev. Lett.* **1988**, *60* (25), 2645–2648. https://doi.org/10.1103/PhysRevLett.60.2645.

(26) Takahata, K.; Iguchi, Y.; Tanaka, D.; Itoh, T.; Terasaki, I. Low Thermal Conductivity of the Layered Oxide Another Example of a Phonon Glass and an Electron Crystal. *Phys. Rev. B - Condens. Matter Mater. Phys.* **2000**, *61* (19), 12551–12555. https://doi.org/10.1103/PhysRevB.61.12551.

(27) Ohta, H.; Nomura, K.; Orita, M.; Hirano, M.; Ueda, K.; Suzuki, T.; Ikuhara, Y.; Hosono, H. Single-Crystalline Films of the Homologous Series $InGaO_3(ZnO)_m$ Grown by Reactive Solid-Phase Epitaxy. *Adv. Funct. Mater.* **2003**, *13* (2), 139–144. https://doi.org/10.1002/adfm.200390020.

(28) Lee, K. H.; Kim, S. W.; Ohta, H.; Koumoto, K. Ruddlesden-Popper Phases as Thermoelectric Oxides: Nb-Doped $SrO(SrTiO_3)_n$ ($n$ = 1, 2). *J. Appl. Phys.* **2006**, *100* (6), 063717. https://doi.org/10.1063/1.2349559.

(29) Jo, I.; Pettes, M. T.; Kim, J.; Watanabe, K.; Taniguchi, T.; Yao, Z.; Shi, L. Thermal Conductivity and Phonon Transport in Suspended Few-Layer Hexagonal Boron Nitride. *Nano Lett.* **2013**, *13* (2), 550–554. https://doi.org/10.1021/nl304060g.

(30) Uematsu, Y.; Terada, T.; Sato, K.; Ishibe, T.; Nakamura, Y. Low Thermal Conductivity in Single Crystalline Epitaxial Germanane Films. *Appl. Phys. Express* **2020**, *13* (5), 055503. https://doi.org/10.35848/1882-0786/ab8726.

(31) Andersson, S.; Collén, B.; Kuylenstierna, U.; Magnéli, A. Phase Analysis Studies on the Titanium-Oxygen System. *Acta Chem. Scand.* **1957**, *11*, 1641–1652. https://doi.org/10.3891/acta.chem.scand.11-1641.

(32) Anderson, J. S.; Hyde, B. G. On the Possible Role of Dislocations in Generating Ordered and Disordered Shear Structures. *J. Phys. Chem. Solids* **1967**, *28* (8), 1393–1408. https://doi.org/10.1016/0022-3697(67)90268-5.

(33) Harada, S.; Tanaka, K.; Inui, H. Thermoelectric Properties and Crystallographic Shear Structures in Titanium Oxides of the Magǹli Phases. *J. Appl. Phys.* **2010**, *108* (8), 083703. https://doi.org/10.1063/1.3498801.

(34) Le Page, Y.; Strobel, P. Structural Chemistry of the Magnéli Phases $Ti_nO_{2n-1}$, $4 \leq n \leq 9$. II. Refinements and Structural Discussion. *J. Solid State Chem.* **1982**, *44* (2), 273–281. https://doi.org/10.1016/0022-4596(82)90374-7.

(35) Bursill, L. A.; Hyde, B. G. Crystal Structures in the {l-32} CS Family of Higher Titanium Oxides $Ti_nO_{2n-1}$. *Acta Crystallogr. Sect. B Struct. Crystallogr. Cryst. Chem.* **1971**, *27* (1), 210–215. https://doi.org/10.1107/s0567740871001912.

(36) Teramoto, T.; Takai, Y.; Hashiguchi, H.; Okunishi, E.; Tanaka, K. Distribution of Alloying Quadrivalent Zirconium in $TiO_{2-x}$ Magnèli Phase. *Mater. Trans.* **2019**, *60* (10), 2199–2203. https://doi.org/10.2320/matertrans.MT-M2019155.

(37) Chen, G. Thermal Conductivity and Ballistic-Phonon Transport in the Cross-Plane Direction of Superlattices. *Phys. Rev. B - Condens. Matter Mater. Phys.* **1998**, *57* (23), 14958–14973. https://doi.org/10.1103/PhysRevB.57.14958.

(38) Lim, J.; Hippalgaonkar, K.; Andrews, S. C.; Majumdar, A.; Yang, P. Quantifying Surface Roughness Effects on Phonon Transport in Silicon Nanowires. *Nano Lett.* **2012**, *12* (5), 2475–2482. https://doi.org/10.1021/nl3005868.

(39) Ong, Z. Y.; Schusteritsch, G.; Pickard, C. J. Structure-Specific Mode-Resolved Phonon Coherence and Specularity at Graphene Grain Boundaries. *Phys. Rev. B* **2020**, *101* (19), 195410. https://doi.org/10.1103/PhysRevB.101.195410.

(40) Ziman, J. M. *Electrons and Phonons*; Clarendon: Oxford, 1960.

(41) Traylor, J. G.; Smith, H. G.; Nicklow, R. M.; Wilkinson, M. K. Lattice Dynamics of Rutile. *Phys. Rev. B* **1971**, *3* (10), 3457–3472. https://doi.org/10.1103/PhysRevB.3.3457.

(42) Sikora, R. Ab Initio Study of Phonons in the Rutile Structure of $TiO_2$. *J. Phys. Chem. Solids* **2005**, *66* (6), 1069–1073. https://doi.org/10.1016/j.jpcs.2005.01.007.

(43) Chen, G. Size and Interface Effects on Thermal Conductivity of Superlattices and Periodic Thin-Film Structures. *J. Heat Transfer* **1997**, *119* (2), 220–229. https://doi.org/10.1115/1.2824212.

(44) Aksamija, Z.; Knezevic, I. Thermal Conductivity of $Si_{1-x}Ge_x/Si_{1-y}Ge_y$ Superlattices: Competition between Interfacial and Internal Scattering. *Phys. Rev. B - Condens. Matter Mater. Phys.* **2013**, *88* (15), 155318. https://doi.org/10.1103/PhysRevB.88.155318.

(45) Ok, K. M.; Ohishi, Y.; Muta, H.; Kurosaki, K.; Yamanaka, S. Effect of Point and Planar Defects on Thermal Conductivity of $TiO_{2-x}$. *J. Am. Ceram. Soc.* **2018**, *101* (1), 334–346. https://doi.org/10.1111/jace.15171.

Table 1. Identified phases and corresponding spacing of the CS planes.

| *n* | Phases | O/Ti | $D_{CS}$ (nm) |
|---|---|---|---|
| 26 | $Ti_{26}O_{51}$ | 1.962 | 2.64 |
| 27 | $Ti_{27}O_{53}$ | 1.963 | 2.75 |
| 28 | $Ti_{28}O_{55}$ | 1.964 | 2.85 |

Table 2. Statistical data for the values of *n* and the interplanar distance of the CS plane for $Ti_{26}O_{51}$, $Ti_{27}O_{53}$ and $Ti_{28}O_{55}$. *N* is the number of measurements.

| Phase | *N* | Standard deviation | |
|---|---|---|---|
| | | *n* | Length (nm) |
| $Ti_{26}O_{51}$ | 63 | 0.37 | 0.039 |
| $Ti_{27}O_{53}$ | 70 | 0.40 | 0.041 |
| $Ti_{28}O_{55}$ | 40 | 0.16 | 0.016 |
| Total | 173 | 0.35 | 0.036 |

Table 3. Ratio of the CS planes with and without site splitting and the estimated values of $R_a$.

| | Ratio (%) | $R_a$ (pm) |
|---|---|---|
| W/O split | 93.3 | 13 |
| W/ split | 6.7 | 39 |
| Average | | 15 |

Table 4. Periodicity and interface roughness for various superlattices and phononic crystals.

| System | Periodicity (nm) | Interface roughness (pm) |
|---|---|---|
| $Ti_nO_{2n-1}$ (this study) | 2.64-2.85 | 15 |
| Si/Ge (CVD)[44] | 3-15 | 120-500 |
| GaAs/AlAs (MBE)[43] | 5-100 | 300-900 |
| AlN/GaN (MBE)[17] | 5 | 70 |
| Si phononic crystal[11] | 300 | 3000 |

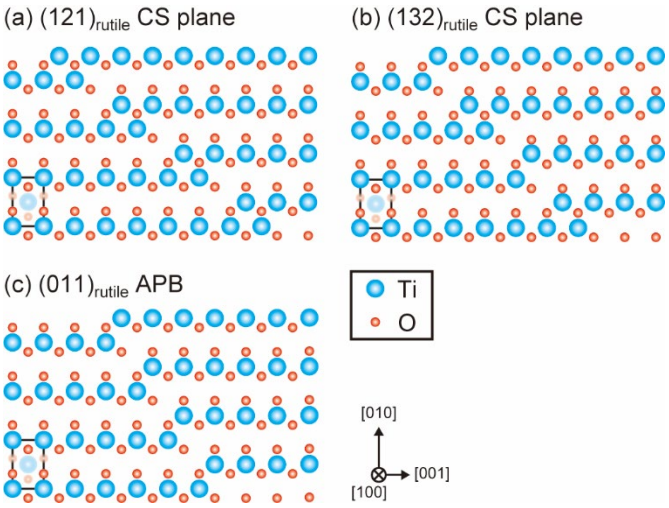


Figure 1. Schematic illustration of the ideal atomic arrangement of titanium oxides with (a) the $(121)_{rutile}$ and (b) the $(132)_{rutile}$ CS planes as well as (c) the $(011)_{rutile}$ APB with the displacement of $1/2[0\text{-}11]_{rutile}$.

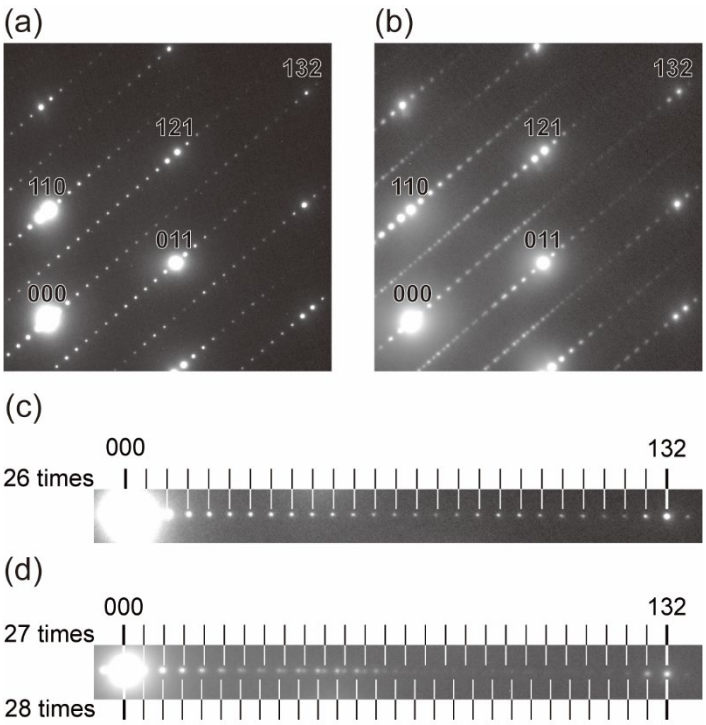


Figure 2. (a)(b) SAED patterns taken from the prepared specimen along the $[1\text{-}11]_{rutile}$ direction with different positions and (c)(d) corresponding magnified images. A line of superlattice spots along $132_{rutile}$ corresponding to $n$ = 26, 27 and 28 periodicity was observed.

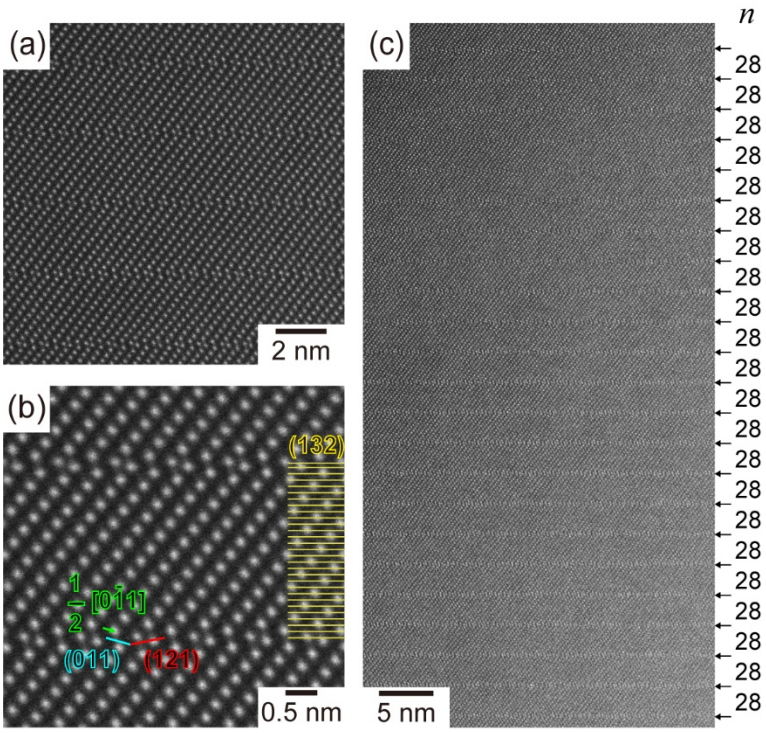


Figure 3. HAADF-STEM images taken along the [1-11]$_{rutile}$ direction. Magnified image of (b) was averaged over 8 different positions. Bright spots corresponding to the titanium atom column and the arrangement of the titanium atom column deviated at the position of the CS planes. In the magnified image (b), the spacing of the CS plane can be evaluated by counting the number of the titanium atom (132) $_{rutile}$ layers. The distribution of the spacing for the CS planes was evaluated in low-magnification images (c).

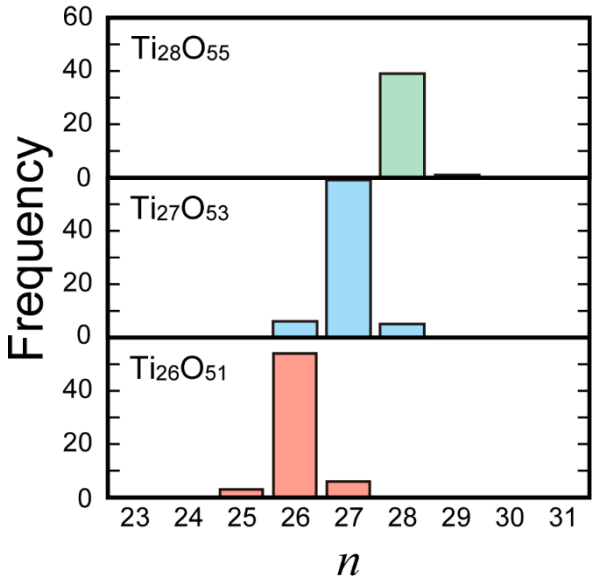


Figure 4. Histogram of the distribution of the values of n for $Ti_{26}O_{51}$, $Ti_{27}O_{53}$ and $Ti_{28}O_{55}$.

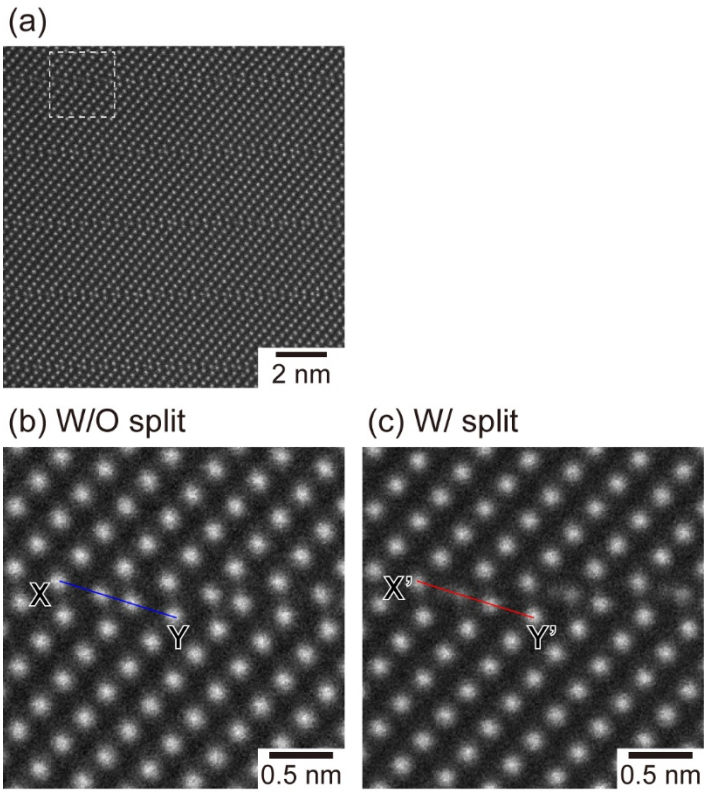


Figure 5. (a) HAADF-STEM image containing split sites on the CS plane. Dashed square indicates the position of split sites. Magnified HAADF-STEM images averaged over 8 different positions of (b) without containing a split site and (c) with split sites.

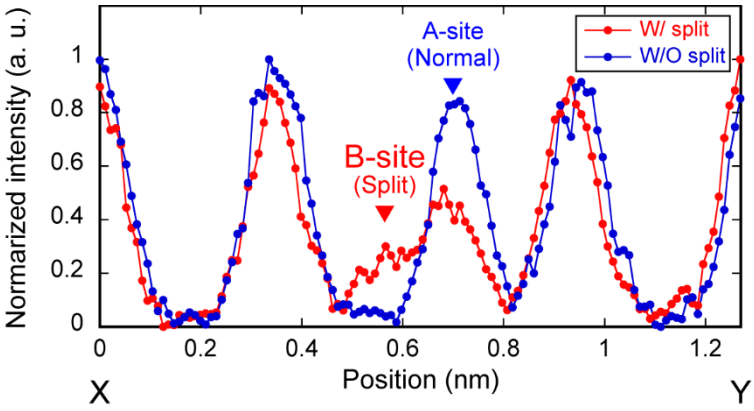


Figure 6. Line profile between X (X') and Y (Y') in Fig. 5(b) without site splitting and 5(c) with site splitting.

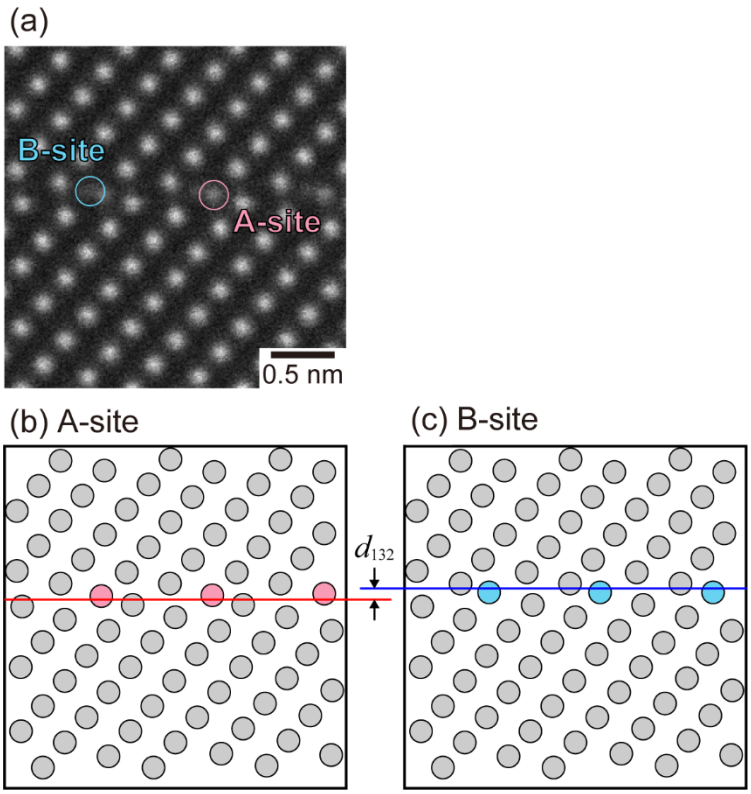


Figure 7. (a) Magnified HAADF-STEM image with site splitting shown in Fig. 5(c) again, and schematic illustration of titanium atomic column site with (b) A-site and (c) B-site. The difference between the two titanium atomic arrangements is the position of the CS planes separated by one $(132)_{rutile}$ spacing.

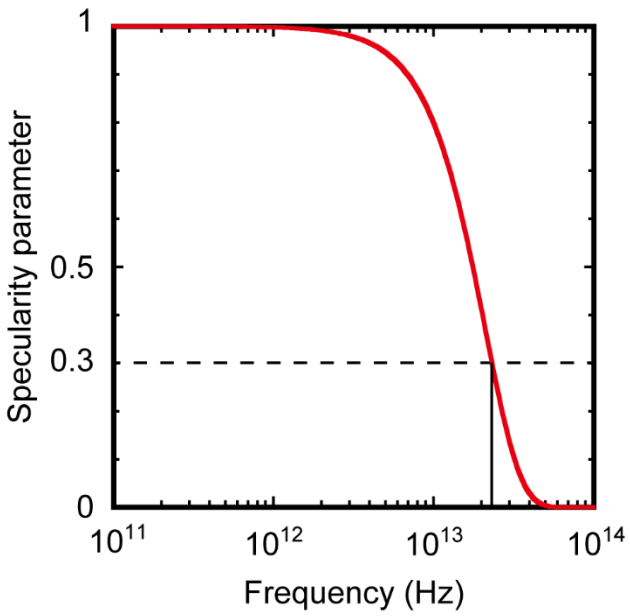


Figure 8. Specularity parameter depending on frequency calculated by Eq. (2) with $R$ = 23 pm for the estimated roughness from STEM observation and $v = 6.1 \times 10^3$ m/s for the average sound velocity of polycrystalline rutile reported by Ok et al[45].